Stochastic properties of auditory brainstem coincidence detectors in binaural perception

Ram Krips and Miriam Furst[a)]
Department of Electrical Engineering-Systems, Faculty of Engineering, Tel-Aviv University, Tel-Aviv 69978, Israel

(Received 25 May 2008; revised 10 December 2008; accepted 11 December 2008)

In the mammalian auditory brainstem, two types of coincidence detector cells are involved in binaural localization: excitatory-excitatory (EE) and excitatory-inhibitory (EI). Using statistics derived from EE and EI spike trains, binaural discrimination abilities of single tones were predicted. The minimum audible angle (MAA), as well as the just noticeable difference of interaural time delay (ITD) and interaural level difference (ILD) were analytically derived for both EE and EI cells on the basis of two possible neural coding patterns, rate coding that ignores a spike's timing information and all-information coding (AIN), which considers a spike's timing occurrences. Simulation results for levels below saturation were qualitatively compared to experimental data, which yielded the following conclusions: (1) ITD is primarily estimated by EE cells with AIN coding when the ipsilateral auditory input exhibits phase delay between 40° and 65°. (2) In ILD, both AIN and rate coding provide identical performances. It is most likely that ILD is primarily estimated by EI cells according to rate coding, and for ILD the information derived from the spikes' timing is redundant. (3) For MAA estimation, the derivation should take into account ambiguous directions of a source signal in addition to its true value.
© *2009 Acoustical Society of America.* [DOI: 10.1121/1.3068446]

PACS number(s): 43.64.Bt, 43.66.Pn, 43.66.Ba, 43.66.Qp [BLM] Pages: 1567–1583

I. INTRODUCTION

Three main acoustic cues are known to contribute to sound localization: interaural time difference (ITD), interaural level difference (ILD), and spectral cues (e.g., review Blauert, 1997; Searle *et al.*, 1976). Systematic psychoacoustical experiments have determined the ability of human beings to spatially localize sounds as well as the capability for detecting acoustical cues. In such experiments, for example, subjects were introduced with two discrete and temporally nonoverlapping sounds from different positions; subjects were required to indicate whether the second sound was to the left or right of the first. Since the mid-20th century, just noticeable difference (JND) of ITD and ILD and the minimum audible angle (MAA) of localization were obtained (Klumpp and Eady, 1956; Zwislocki and Feldman, 1956; Mills, 1958; Mills, 1960; Grantham, 1986).

Most studies that tried to model the ability to lateralize a perceived signal were based on the existence of coincidence detectors (CDs) (Jeffress, 1948). The CD based model that Jeffress developed was founded on three main assumptions: bilateral time-locked (phase-locked) inputs into the ITD-processing system, coincidence detection by ITD detector neurons, and an arrangement of delay lines to adjust CD neurons to different preferred ITDs, creating azimuthally a topographic representation of space.

Physiological studies have shown that many cells in the auditory midbrain are sensitive to the direction of sound sources (King and Palmer, 1983; Knudsen, 1982; Knudsen and Konishi, 1978; Semple *et al.*, 1983; see Irvine, 1992, for a review).

The initial processing of interaural timing cues occurs in the medial superior olive (MSO) in which neurons tuned for low-frequency sounds are relatively overrepresented in comparison to neurons tuned to high frequencies. MSO neurons receive excitatory input from the large spherical bushy cells of both (right and left) antro ventral cochlear nucleus (AVCN), which preserve and even enhance the timing accuracy seen in the auditory nerve providing exquisitely timed inputs (Warr, 1966, 1969; Palmer *et al.*, 2002; Joris *et al.*, 1994).

The initial processing of ILDs occurs in the lateral superior olive (LSO) where high-frequency neurons are relatively over-represented compared to low-frequency neurons. The small spherical bushy cells of the ipsilateral AVCN form excitatory synapses on LSO principal neurons (Warr, 1966; Glendenning *et al.*, 1985; Cant, 1991). Additionally, LSO neurons receive inhibitory inputs from neurons in the ipsilateral medial nucleus of the trapezoid body (MNTB), which, in turn, receive excitatory input from the globular bushy cells of the contralateral cochlear nucleus (Glendenning *et al.*, 1985; Cant, 1991; Warr, 1972; Boudreau and Tsuchitani, 1968). The pathway from VCN to MNTB is characterized by synapses producing secure short-latency responses and, therefore, near coincident arrival at the LSO of the ipsilateral excitation and the contralateral inhibition. Neurons in the LSO are sensitive to the balance of intensity at the ears because the excitation due to ipsilateral sounds is reduced by

[a)]Author to whom correspondence should be addressed. Electronic mail: mira@eng.tau.ac.il

increasing levels of contralateral sounds (Boudreau and Tsuchitani, 1970; Guinan *et al.*, 1972; Caird and Klinke, 1983; Caspary and Finlayson, 1991).

Cells that are sensitive to localization cues such as ITD and ILD were identified in both the superior olivary complex (SOC) and the inferior colliculus (IC) (Goldberg and Brown, 1969; Rose *et al.*, 1967; Irvine, 1986, 1992; Delgutte *et al.*, 1999; Fitzpatrick *et al.*, 2000). There are mainly two types of cells that are sensitive to binaural cues: excitatory-excitatory (EE) cells and excitatory-inhibitory (EI) cells (Rose *et al.*, 1967; Goldberg and Brown, 1969; Yin *et al.*, 1987; Yin and Chan, 1990; Joris and Yin, 1995; Joris, 1996; Batra *et al.*, 1997; Palmer *et al.*, 1997; McAlpine *et al.*, 1998; Brand *et al.*, 2002).

Mammalian EE and EI cells are natural candidates for CDs in a "Jeffress-type" system (Moushegian *et al.*, 1975; Yin and Chan, 1990; Joris *et al.*, 1998). The evidence to support this view includes the connection patterns with excitatory inputs from both sides, the cyclic nature of the ITD sensitivity when tested with pure tones, and the fact that the best ITD could be predicted on the basis of the time delay of the response to the monaural inputs from both ears (Goldberg and Brown, 1969; Crow *et al.*, 1978; Yin and Chan, 1990; Spitzer and Semple, 1995). Moreover, results from many human psychophysical studies can be explained by the concept of binaural cross correlation, as indicated by the Jeffress model (Stern and Trahiotis, 1995; Palmer *et al.*, 2002). Most published models for ITD are based on EE cells (review by Colburn, 1996). Yet, recent models account for some aspects of the binaural ITD phenomena with EI cells (e.g., McAlpine *et al.*, 1998; Colburn *et al.*, 2004). ILD processing is frequently considered and modeled by EI mechanisms (Lindemann, 1986; Breebaart, 2001; Yue and Johnson, 1997; Park *et al.*, 2004).

In modeling experimental JND, it is assumed that the neural system estimates the measured parameter (α), and if the brain is acting as an optimal estimator, then the JND is equal to the standard deviation of the estimator (Siebert, 1968). Moreover, if the estimator is unbiased, its variance is bounded by the Cramer–Rao lower bound (CRLB).

A CRLB has been derived for an auditory nerve fiber that behaves as a nonhomogeneous Poisson process (NHPP) where the timing of the spikes was considered (Bar David, 1969). Even though the CRLB derivation yielded significantly lower values than human experimental performance (Siebert, 1968; Colburn, 1973; Heinz *et al.*, 2001), it was generally found to be very useful in indicating constraints in models of the auditory system. For example, calculation of frequency JND as a function of the stimulus frequency and signal duration indicated that rate coding is insufficient for explaining experimental data (Heinz *et al.*, 2001).

Some previous studies predicted binaural psychoacoustical properties by deriving lower bounds of the neural activity. In some studies, CRLBs of the two monaural auditory nerves followed by theoretical coincident detectors were derived (Colburn, 1973; Stern and Colburn, 1978; Huettel and Collins, 2004; Cohen *et al.*, 2004). In other studies, such as Yue and Johnson (1997), specific LSO cells' response was presented as a function of the binaural stimuli. Those cells are mainly response to high frequencies where there is no phase synchronization. An optimal decision model was applied to the LSO's cells response that yielded a biased bound.

We have recently proven that the outputs of both EE and EI cells, whose inputs behave as NHPP, also behave as NHPP, and their corresponding instantaneous rates (IRs) were analytically derived (Krips, 2008). In the present paper, we are using our recent theoretical result in order to predict psychoacoustical binaural discrimination abilities. None of the previous studies could determine analytically the lower bounds from the neural activity of EE and EI cells. These analytic derivations allow us to compare EE and EI performances in detecting binaural cues according to both types of coding, rate coding and all-information coding (AIN).

II. THEORETICAL METHODOLOGY

A. Derivation of JND lower bounds on the basis of neural activity

In a psychoacoustical experiment that was designed to detect the minimal perceived difference of a parameter α, JND(α) is obtained. In modeling such an experiment, we assume that the brain acts as an unbiased optimal estimator, which yields for $\alpha=\alpha^*$ the estimator $\hat{\alpha}$ that satisfies the following conditions (Hartmann and Rakerd, 1989):

$$E[\hat{\alpha}] = \alpha^*,$$

$$\mathrm{JND}(\alpha^*) \approx \sigma(\hat{\alpha}) \geqslant \mathrm{CRLB}(\alpha^*), \tag{1}$$

where CRLB(α^*) is the CRLB at $\alpha=\alpha^*$.

When the estimation is based on a neural activity that behaves as NHPP, there are two possible ways to analyze the performance. The first way is referred to as "rate coding," which means that the performance is analyzed on the basis of the number of spikes that yields a stimulus during an interval of length T s. The probability density function (pdf) is obtained by

$$P_{\mathrm{rate}}(N(0,T)=n) = \frac{1}{n!}\left[\int_0^T \lambda(t,\alpha)dt\right]^n \times \exp\left\{-\int_0^T \lambda(t,\alpha)dt\right\}, \tag{2}$$

where $\lambda(t,\alpha)$ is the IR of the nerve fiber. The resulting CRLB is obtained by (Snyder and Miller, 1991)

$$\mathrm{CRLB}_{\mathrm{rate}}(\alpha^*) = \frac{1}{\sqrt{\frac{T}{\bar{\lambda}(\alpha^*)}\left[\left.\frac{\partial\bar{\lambda}(\alpha)}{\partial\alpha}\right|_{\alpha=\alpha^*}\right]^2}}, \tag{3}$$

where $\bar{\lambda}(\alpha)=(1/T)\int_0^T\lambda(t,\alpha)dt$ is the average rate.

For AIN the timing of discharge spikes is considered in addition to the number of spikes in the interval, which yields the following pdf:

$$P_{\mathrm{AIN}}(t_1,\ldots,t_n)=\frac{1}{n!}\prod_{k=1}^{n}\lambda(t_k,\alpha)\exp\left\{-\int_0^T\lambda(t,\alpha)dt\right\}, \tag{4}$$

where $t_1,\ldots,t_n$ are the discharge times. The resulting CRLB was derived by Bar David (1969), which yields

$$\mathrm{CRLB}_{\mathrm{AIN}}(\alpha^*)=\frac{1}{\sqrt{\int_0^T\frac{1}{\lambda(t,\alpha^*)}\left[\left.\frac{\partial\lambda(t,\alpha)}{\partial\alpha}\right|_{\alpha=\alpha^*}\right]^2dt}}. \tag{5}$$

CRLB is useful when the estimator uses information from the vicinity of the true value α^*. However, there are cases where the estimator might use other values besides the true one. For example, a subject will similarly perceive a continuous 2 kHz tone that originated from his right side, left side, or the front of his head (e.g., Kuhn, 1987). Thus, when the brain estimates the direction of such a tone, all these possibilities should be considered. CRLB in such cases is inadequate (Krips and Furst, 2006a).

Barankin (1949) developed a lower bound that takes into account different possible values of the estimated parameter other than those located in the proximity of the true one (ambiguous locations). If the true value is α^* and there are L other possible values, $\alpha_1,\ldots,\alpha_L\neq\alpha^*$, then the Barankin lower bound (BLB) was derived (McAulay and Hofstetter, 1971) and is obtained by

$$\begin{aligned}\sigma(\hat{\alpha})&\geqslant\mathrm{BLB}(\alpha^*)\\&=\sqrt{[\mathrm{CRLB}(\alpha^*)]^2+\underline{\Gamma}(\alpha^*)\Delta^{-1}(\alpha^*)\underline{\Gamma}^T(\alpha^*)},\end{aligned} \tag{6}$$

where $\underline{\Gamma}(\alpha^*)=\underline{\alpha}-\mathrm{CRLB}^2(\alpha^*)\underline{A}$ and $\Delta(\alpha^*)=B-\underline{A}^T\mathrm{CRLB}^2(\alpha^*)\underline{A}$. $\mathbf{B}$ is a symmetric matrix whose size is $L\times L$ and the $\underline{\alpha}$ and $\underline{A}$ are vectors whose size are L ($\underline{\alpha}=[\alpha_1,\ldots,\alpha_L]$, $\underline{A}=[A_1,\ldots,A_L]$). The vector $\underline{A}$ and the matrix $\mathbf{B}$ are derived in Appendix A (Krips, 2008) for both rate coding [Eq. (2)] and AIN [Eq. (4)], which yields

$$\begin{aligned}A_i^{\mathrm{rate}}&=T\left.\frac{\partial\bar{\lambda}(\alpha)}{\partial\alpha}\right|_{\alpha=\alpha^*}\left[\frac{\bar{\lambda}(\alpha_i)}{\bar{\lambda}(\alpha^*)}-1\right],\quad i=1,\ldots,L,\\A_i^{\mathrm{AIN}}&=\int_0^T\left.\frac{\partial\lambda(t,\alpha)}{\partial\alpha}\right|_{\alpha=\alpha^*}\left[\frac{\lambda(t,\alpha_i)}{\lambda(t,\alpha^*)}-1\right]dt,\quad i=1,\ldots,L\end{aligned} \tag{7}$$

and

$$\begin{aligned}B_{i,j}^{\mathrm{rate}}&=\exp\left\{-T\left[\bar{\lambda}(\alpha_i)+\bar{\lambda}(\alpha_j)-\bar{\lambda}(\alpha^*)-\frac{\bar{\lambda}(\alpha_i)\bar{\lambda}(\alpha_j)}{\bar{\lambda}(\alpha^*)}\right]\right\},\\B_{i,j}^{\mathrm{AIN}}&=\exp\left\{-\int_0^T\left[\lambda(t,\alpha_i)+\lambda(t,\alpha_j)-\lambda(t,\alpha^*)-\frac{\lambda(t,\alpha_i)\lambda(t,\alpha_j)}{\lambda(t,\alpha^*)}\right]dt\right\}\end{aligned} \tag{8}$$

for $i,j=1,\ldots,L$.

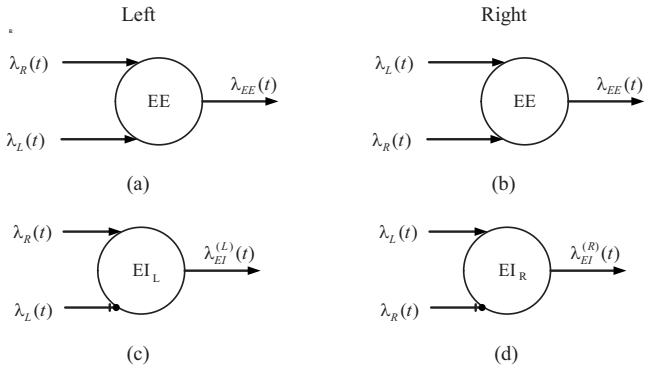

FIG. 1. Schematic description of (a) left SOC EE cell, (b) right SOC EE cell, (c) left SOC EI cell, and (d) right SOC EI cell. The inputs are from the right and left auditory nerves that are indicated by their IRs $\lambda_R(t)$ and $\lambda_L(t)$, respectively. Excitatory input is indicated by an arrow, and an inhibitory input by a black circle.

B. Derivation of EE and EI cell instantaneous rates

In this paper we investigate the ability of CD cells to predict psychoacoustical binaural abilities. We particularly refer to two typical CD cells, EE and EI, that are found in both the right and left mammalian SOCs (see Fig. 1). Each input represents a single primarylike auditory nerve that statistically behaves as NHPP.

EE cells receive two inputs [Figs. 1(a) and 1(b)] that arrive from the two ears. The IRs of the right and left inputs are denoted by $\lambda_R(t,\alpha)$ and $\lambda_L(t,\alpha)$, and their correspondent refractory periods are represented by τ_R and τ_L, respectively. We showed that if the two inputs behave as NHPP and if the time interval (Δ) in which the two inputs can interact satisfies the condition $\Delta\ll\min\{\tau_R,\tau_L\}$, then EE output also behaves as NHPP and its IR is obtained by

$$\begin{aligned}\lambda_{\mathrm{EE}}(t,\alpha)&=\lambda_L(t,\alpha)\int_{t-\Delta}^{t}\lambda_R(t',\alpha)dt'\\&\quad+\lambda_R(t,\alpha)\int_{t-\Delta}^{t}\lambda_L(t',\alpha)dt'.\end{aligned} \tag{9}$$

Since both right and left EE cells receive similar inputs, their output IR is also identical, i.e.,

$$\lambda_{\mathrm{EE}}^{(R)}(t,\alpha)=\lambda_{\mathrm{EE}}^{(L)}(t,\alpha)=\lambda_{\mathrm{EE}}(t,\alpha). \tag{10}$$

A possible coincidence window is $\Delta=20$ μs (Agmon-Snir *et al.* 1998). It was previously used in theoretical models (e.g., Colburn, 1973; Heinz *et al.*, 2001; Cohen, *et al.*, 2004). This value satisfies the condition $\Delta\ll\min\{\tau_R,\tau_L\}$ since the refractory period at the auditory nerve is of the order of 500 μs to 1 ms (Miller *et al.*, 2001; Dynes, 1996; Bruce *et al.*, 1999; Brown and Abbas, 1990).

EI cells receive two types of inputs, an excitatory input and an inhibitory input. The EI in the right SOC [Fig. 1(d)] receives an excitatory input from the left side and an inhibitory input from the right side, which yield

$$\lambda_{\mathrm{EI}}^{(R)}(t,\alpha)=\lambda_L(t,\alpha)\left(1-\int_{t-\Delta}^{t}\lambda_R(t',\alpha)dt'\right). \tag{11}$$

On the other hand, EI cells in the left SOC receive the antisymmetric inputs, i.e., an excitatory input from the right side and an inhibitory input from the left side [Fig. 1(c)], which yield

$$\lambda_{\mathrm{EI}}^{(L)}(t,\alpha)=\lambda_R(t,\alpha)\left[1-\int_{t-\Delta}^{t}\lambda_L(t',\alpha)dt'\right]. \tag{12}$$

A possible coincidence window is $\Delta=200\ \mu$s (Park, 1998). It is ten times longer than found in EE cells. However it satisfies the condition $\Delta<\min\{\tau_R,\tau_L\}$, which guarantees that EI cells behave as NHPP if their inputs also behave as NHPP.

C. Prediction of JND on the basis of both SOCs

In order to predict the psychoacoustical results, for every type of cell EE or EI, both sides are combined. This yields bounds of each side that provides

$$\begin{aligned}\mathrm{JND}_{\mathrm{EE}}(\alpha^*)&=1/\sqrt{[\mathrm{CRLB}_{\mathrm{EE}}^{(R)}(\alpha^*)]^{-2}+[\mathrm{CRLB}_{\mathrm{EE}}^{(L)}(\alpha^*)]^{-2}},\\ \mathrm{JND}_{\mathrm{EI}}(\alpha^*)&=1/\sqrt{[\mathrm{CRLB}_{\mathrm{EI}}^{(R)}(\alpha^*)]^{-2}+[\mathrm{CRLB}_{\mathrm{EI}}^{(L)}(\alpha^*)]^{-2}},\end{aligned} \tag{13}$$

where $\mathrm{CRLB}_{\mathrm{EE}}^{(R)}(\alpha^*)$, $\mathrm{CRLB}_{\mathrm{EI}}^{(R)}(\alpha^*)$, $\mathrm{CRLB}_{\mathrm{EE}}^{(L)}(\alpha^*)$, and $\mathrm{CRLB}_{\mathrm{EI}}^{(L)}(\alpha^*)$ are the CRLBs obtained by EE and EI cells in the right and left SOCs, respectively.

D. Derivation scheme for binaural simple tones

In this paper we test localization abilities that are evoked by audio signal $S(t,\theta)$ that enters both ears from direction θ. The incoming sounds to each ear are transformed in ways which depend on the shape and size of the head, torso, and the outer ears' pinna. These anatomical features are known as the head related transfer function (HRTF) that can be measured and synthesized in the form of linear time-invariant filters. Therefore, the signals that are conveyed to the left and right cochleae are

$$\begin{aligned}S_L(t,\theta)&=S(t,\theta)*\mathrm{HRTF}_L(t,\theta),\\ S_R(t,\theta)&=S(t,\theta)*\mathrm{HRTF}_R(t,\theta),\end{aligned} \tag{14}$$

where $*$ represents a convolution, and $\mathrm{HRTF}_L(t,\theta)$ and $\mathrm{HRTF}_R(t,\theta)$ are the left and right HRTFs.

This paper presents only the tests of signals that are composed of simple tones, i.e., $S(t)=A\sin(2\pi ft)$. The effects of the HRTF on such a signal are a phase shift and amplitude alteration, which yield

$$\begin{aligned}S_L(t,\theta)&=A_L(\theta)\sin(2\pi ft+\varphi_L(\theta)),\\ S_R(t,\theta)&=A_R(\theta)\sin(2\pi ft+\varphi_R(\theta)).\end{aligned} \tag{15}$$

Therefore the resulting interaural difference is an interaural phase difference (IPD), which is obtained by

$$\mathrm{IPD}(\theta)=\varphi_R(\theta)-\varphi_L(\theta), \tag{16}$$

which corresponds to ITD by

$$\mathrm{ITD}(\theta)=\frac{\mathrm{IPD}(\theta)}{2\pi f}, \tag{17}$$

and the ILD in dB is given by

$$\mathrm{ILD}(\theta)=20\log_{10}\left(\frac{A_R(\theta)}{A_L(\theta)}\right)=20\log_{10}(\delta), \tag{18}$$

where $\delta=A_R(\theta)/A_L(\theta)$.

The IRs of EE and EI cells [Eqs. (9), (11), and (12)] depend on the input IRs $\lambda_L(t)$ and $\lambda_R(t)$. The input fibers to the SOC's EE and EI cells arrive from the CN. We assume that those are primarylike nerves and that their statistical properties are similar to those of the auditory nerve.

The auditory nerve IR for simple tone stimuli is commonly expressed with exponential functions (e.g., Siebert, 1968; Colburn, 1973; Heinz *et al.*, 2001; Cohen *et al.*, 2004) as follows:

$$\begin{aligned}\lambda_L(t)&=\Lambda(S_L(t,\theta))\exp\{B(S_L(t,\theta))\sin(2\pi ft+\varphi_L(\theta)+\Theta_L(f))\},\\ \lambda_R(t)&=\Lambda(S_R(t,\theta))\exp\{B(S_R(t,\theta))\sin(2\pi ft+\varphi_R(\theta)+\Theta_R(f))\}.\end{aligned} \tag{19}$$

Generally, $\Lambda(S(t,\theta))$ is a function of the stimulus level. It has a minimum value that is equal to the fiber's spontaneous rate and a maximum value that represents the fiber's saturation rate. For stimuli whose levels are in the midrange ($20\leqslant A\leqslant 50$ dB SPL), $\Lambda(S(t,\theta))$ is proportional to the stimulus level, i.e., $\Lambda(A\sin(2\pi ft))=\gamma A$. The proportional coefficient (γ) is different for every fiber as determined by the location along the cochlear partition that the fiber innervates. In this paper we refer only to stimuli in the midrange levels, where the IR is proportional to the stimuli level. The function $B(S(t,\theta))$ governs the synchronization of the fiber response, which decreases with the increase in both frequency and level of simple tone stimuli. In this paper we refer only to the dependence of the synchronization on frequency. The synchronization is typically measured by its vector strength (VS), which is obtained by

$$\mathrm{VS}(f)=\frac{\Upsilon(f)}{\Upsilon(0)}, \tag{20}$$

where $\Upsilon(f)$ is the absolute value of the IR's Fourier transform. VS data (Palmer and Russell, 1986; Johnson, 1980; Rose *et al.*, 1967) can be modeled by sigmoid functions such as

$$\mathrm{VS}(f)=2\frac{e^{-\beta\cdot f}}{1+e^{-\beta\cdot f}}. \tag{21}$$

A family of VS function is plotted as a function of frequency in Fig. 2. Each curve was obtained with a different β. The leftmost (unsynchronized) curve in Fig. 2 was obtained with $\beta=0.0007$ and corresponds to species where their auditory nerve fibers start losing their synchrony below 1 kHz (Liu *et al.*, 2006). There are other species that lose their synchrony at higher frequencies; e.g., cats and squirrel monkeys start losing synchrony above 3 kHz (Johnson, 1980; Palmer and Russell, 1986; Rose *et al.*, 1967; Reyes *et al.*, 1996). Thus their VS can be fitted with higher values of β (for example, the smallest value used was of $\beta=0.0001$).

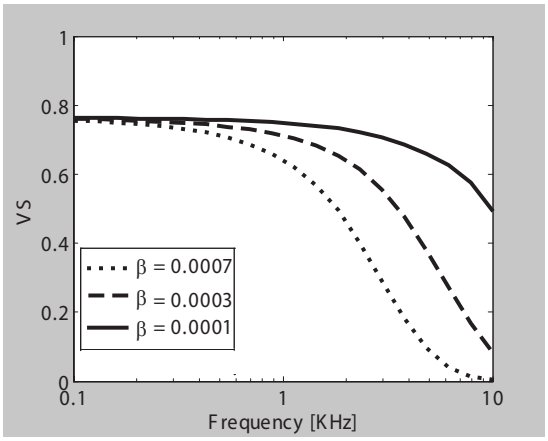

FIG. 2. VS as a function of frequency. Each curve represents a different function [Eq. (21)] as indicated by the parameter β.

III. SIMULATION RESULTS

A. Interaural phase difference

In order to evaluate the ability of EE and EI cells to predict properties that are related to ITD or IPD, the dependence on both the stimulus direction and level is ignored. Therefore,

$$S_L(t) = \sin(2\pi f t), \qquad S_R(t) = \sin(2\pi f t + \mathrm{IPD}). \tag{22}$$

The IRs $\lambda_{EE}^{(R)}(t,\mathrm{IPD})$, $\lambda_{EE}^{(L)}(t,\mathrm{IPD})$, $\lambda_{EI}^{(R)}(t,\mathrm{IPD})$, and $\lambda_{EI}^{(L)}(t,\mathrm{IPD})$ were obtained by substituting Eq. (22) in Eq. (19). Initially we assumed that $\Theta_L(f)=\Theta_R(f)=0$.

Figure 3 represents the normalized average rates $\bar{\lambda}_{EE}$ and $\bar{\lambda}_{EI}$ as a function of IPD for different input frequencies. The input rates were obtained according to Eq. (19) by substituting $\Lambda=200$ spikes/s. The normalization was obtained to the signal period (i.e., for every frequency f, $T=1/f$). We chose to indicate the VS of the fiber rather than its frequency because IR dependence on frequency is uniquely determined by a nerve's synchronization functions $B(S(t,\theta))$ [Eq. (19)]. Moreover, different synchronization functions can yield different frequencies for the same VS, as shown in Fig. 2.

Since both right and left EE cells are identical, the normalized average rate of the output of an EE cell is presented in a single figure [Fig. 3(a)] as a function of IPD. It yields a maximum when both inputs are in phase (IPD=0°) and decreases with an increase in |IPD|. In general, a similar behavior was obtained for all input frequencies. However, for large values of VS, which correspond to low frequencies, a distinct peak is observed; for low VS values that correspond to high frequencies, the mean rate as a function of IPD reveals shallower curves.

In the simulation shown in Fig. 3(a), we used a coincidence window $\Delta=20$ μs. Increasing Δ will cause steeper curves as a function of IPD, but the general behavior holds. It is therefore clear from Fig. 3(a) that EE cells describe an

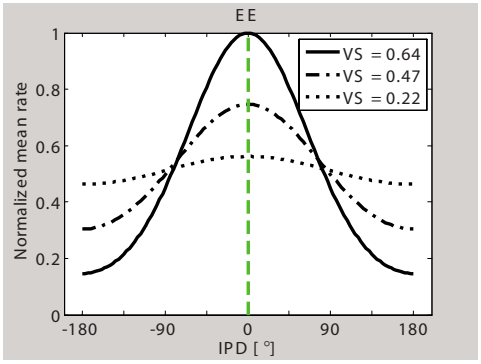

(a)

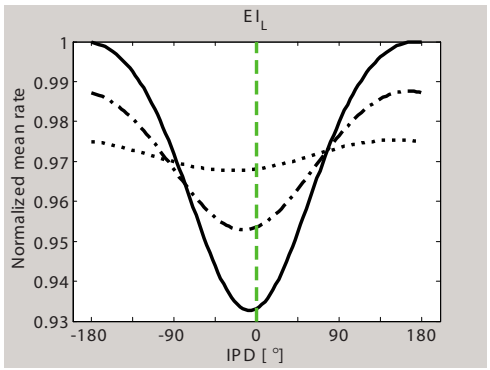

(b)

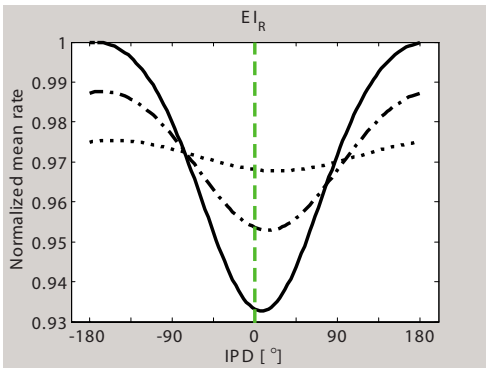

(c)

FIG. 3. (Color online) Normalized mean spiking rate as a function of IPD for different frequencies as indicated by their VS. Each panel represents a different cell: (a) EE, (b) left EI, and (c) right EI cells. Derivation was obtained with the following parameters: $\Lambda=200$ spikes/s for all inputs, $\Delta=20$ μs for EE cell, and $\Delta=200$ μs for EI cell.

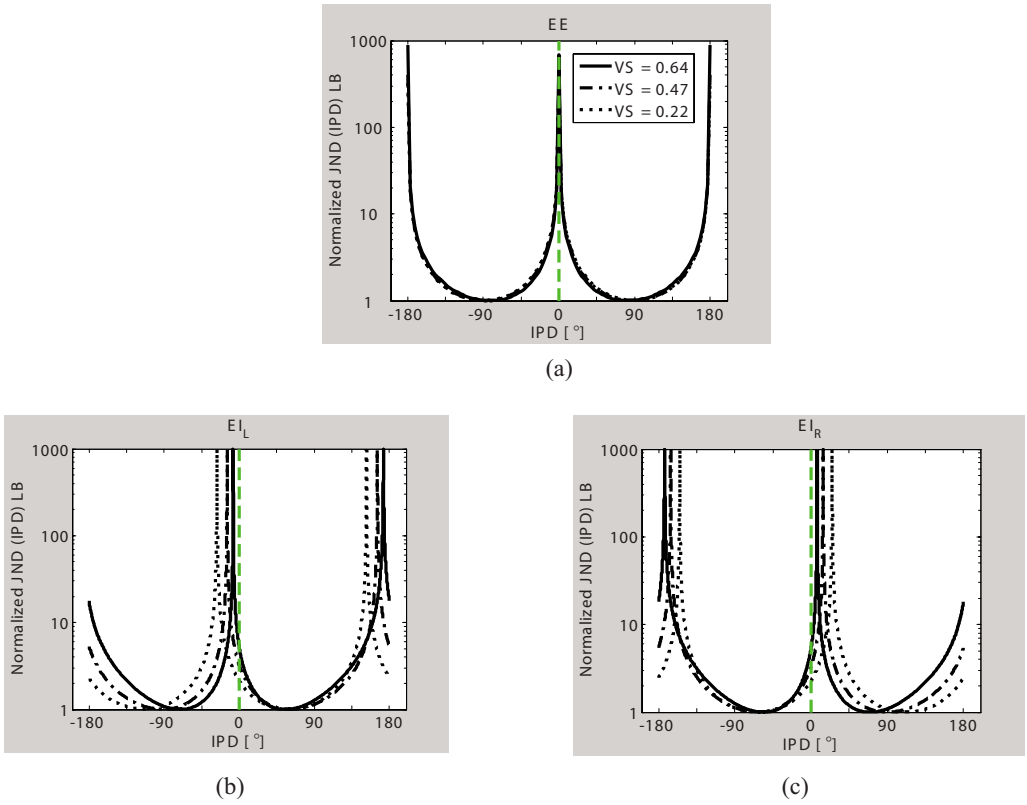

FIG. 4. (Color online) Normalized lower bound of JND of IPD obtained by rate coding as a function of IPD derived by (a) EE cell, (b) left EI cell, and (c) right EI cell. Each curve represents a different input frequency as indicated by its VS.

efficient correlator mechanism between the two ears, especially for frequencies with high VS (low frequencies).

The left and right EI cells are antisymmetric, as can be seen in Fig. 1. The inhibitory input arrives from the ipsilateral ear, while the excitatory input arrives from the contralateral ear. $\bar{\lambda}_{\mathrm{EI}}^{(R)}$ yields a minimum at $\phi=\mathrm{IPD}>0$ [Fig. 3(c)], while $\bar{\lambda}_{\mathrm{EI}}^{(L)}$ reveals a minimum at $-\phi$ [Fig. 3(b)]. In both left and right cases, the minimum rate was obtained when the inhibitory input preceded the excitatory input by $\phi°$. In the simulation for EI cells, we used a coincidence window $\Delta=200\ \mu\mathrm{s}$.

The IRs $\lambda_{\mathrm{EE}}^{(R)}(t,\mathrm{IPD})$, $\lambda_{\mathrm{EE}}^{(L)}(t,\mathrm{IPD})$, $\lambda_{\mathrm{EI}}^{(R)}(t,\mathrm{IPD})$, and $\lambda_{\mathrm{EI}}^{(L)}(t,\mathrm{IPD})$ were used to calculate the CRLB of JND (IPD) according to the rate coding [Eq. (3)] and the AIN coding [Eq. (5)].

Figures 4 and 5 present CRLB (IPD) as a function of IPD, according to both rate coding and AIN, respectively. Since $\lambda_{\mathrm{EE}}^{(R)}(t,\mathrm{IPD})=\lambda_{\mathrm{EE}}^{(L)}(t,\mathrm{IPD})$, both right and left EE cells provide identical behaviors that correspond to EE in Figs. 4(a) and 5(a). Right and left EI cells, on the other hand, provide different behaviors, as can be seen in Figs. 4(b), 4(c), 5(b), and 5(c). Since the maximum value reached infinity, the results were normalized to the minimum value in each figure.

For the rate coding (Fig. 4), EE cells yielded a minima at about $\mathrm{IPD}=\pm 90°$, where the average rate had a maximum derivative [Eq. (3) and Fig. 3]. An infinite bound was obtained for IPD=0°. This behavior was found for all frequencies [Fig. 4(a)]. Both right and left EI cells provided frequency-dependent minima. For example, for frequencies whose $0.22\leqslant \mathrm{VS}\leqslant 0.64$, the minimum CRLB was obtained at $90°\geqslant \mathrm{IPD}\geqslant 60°$, respectively.

The AIN yielded quite a different behavior as a function of IPD (Fig. 5). For EE it yielded for all frequencies, minimum at about $\mathrm{IPD}\approx\pm 50°$ and a local maximum at IPD $=0°$. The right EI cell yielded, for all frequencies, a minimum at about $\mathrm{IPD}\approx 0°$. On the other hand, the left EI cell yielded a global minimum at $\mathrm{IPD}=\pm 180°$ and a local minimum at $\mathrm{IPD}\approx 0°$.

In order to predict the psychoacoustical results, we combined the information from both sides as expressed in Eq. (13). We expect the best performance in the frontal position and symmetric performance in both sides, i.e., a minimum JND at IPD=0° and a symmetric increase in JND with an absolute increase in IPD (Mills, 1958; Durlach and Colburn, 1978). In view of the results in Figs. 3–5, the psychoacoustical measurements are unpredictable from either rate coding or all-information coding. We thus propose to introduce a phase delay in the ipsilateral input of both EE and EI cells, which means introducing $\Theta_L(f)\neq 0$ or $\Theta_R(f)\neq 0$ in Eq. (19) for left or right CD cells, respectively. In order to obtain the actual phase delay that will yield a minimum JND at IPD $=0°$, the lower bound of the binaural JND was computed according to Eq. (13) with different values of $\Theta_L(f)$ and $\Theta_R(f)$. The phase delay that yielded the minimum JND at IPD=0° was chosen as the ipsilateral input phase delay.

Physiological experiments in cats and guinea pigs that measured the average neural response of different cells in the

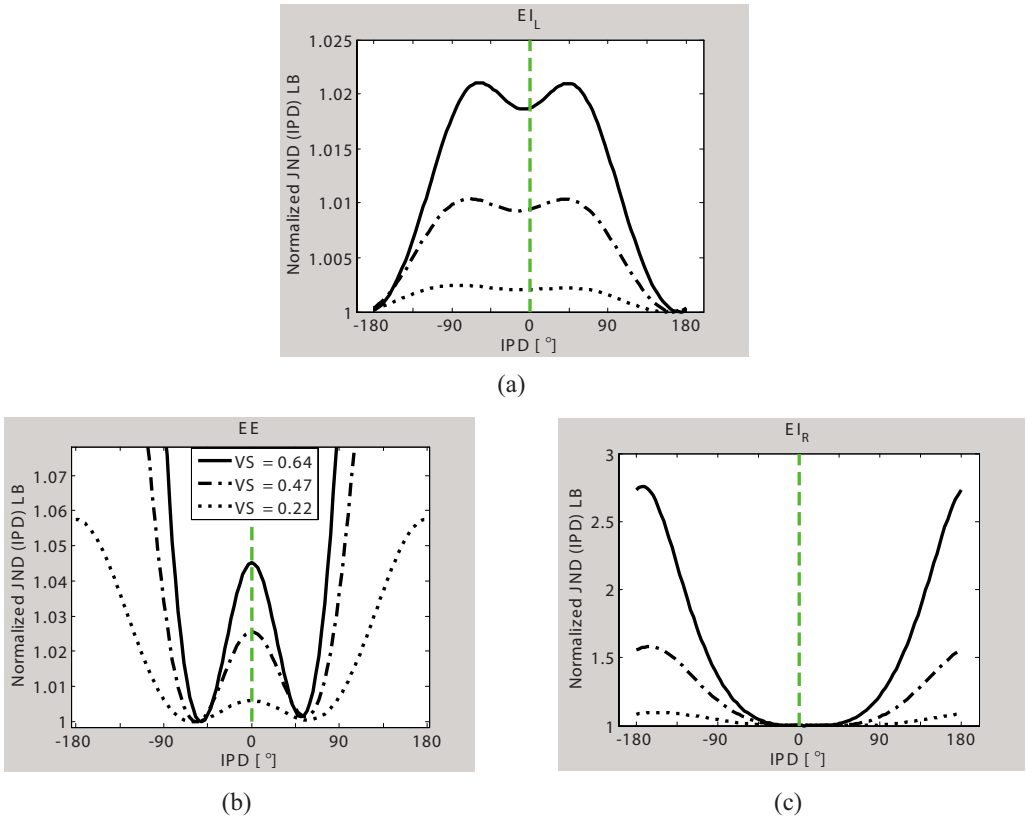

FIG. 5. (Color online) Normalized lower bound of JND of IPD obtained by AIN coding as a function of IPD derived by (a) EE cell, (b) left EI cell, and (c) right EI cell. Each curve represents a different input frequency as indicated by its VS.

IC, whose characteristic frequency was equal to the stimulus frequency, yielded a maximum response at $40° \leqslant \text{IPD} \leqslant 65°$ (Yin and Chan, 1990; Palmer *et al.*, 2002; McAlpine and Grothe, 2003; Hancock and Delgutte, 2004; Joris and Yin, 2006). Low frequencies (below 200 Hz) yielded a maximum response at $\text{IPD} \approx 40°$, while the maximum response at high frequencies (1000–1100 Hz) was obtained at $\text{IPD} \approx 65°$. There was a small monotonic increase in IPD as a function of frequency. One would expect a maximum response at $\text{IPD} \approx 0°$; thus these data are interpreted as having a phase shift between 40° and 65° in the ipsilateral input.

A comparison between the derived ipsilateral phase delay and experimental results is shown in Fig. 6. Derivations were obtained for EE and EI cells according to both types of coding, rate and AIN. The results in Fig. 6 are plotted as a function of VS. The mean experimental data were fitted to a linear regression line, and the measurements' standard deviations were indicated by error bars (McAlpine and Grothe, 2003; Hancock and Delgutte, 2004). The fitted regression lines ± standard deviation are plotted as gray shadowed areas in Fig. 6. There are six panels in Fig. 6; the left panels represent AIN coding, and the right panels represent rate coding. The derivations for EE cells are presented in the upper row, and EI cell derivations are presented in the second and third rows.

Panel (a) in Fig. 6 represents the best input phase delay as derived by EE cell according to AIN coding (solid line). The computed phase delay resembles the experimental results (gray shadowed areas), a moderate decrease in the absolute phase as a function of VS, which means moderate increase as a function of frequency. In none of the other panels, the theoretical derivations (solid lines) resemble the experimental results.

The derived optimal ipsilateral input phase delay was substituted in Eq. (19), the lower bounds of the JND were computed according to Eq. (13), and the normalized values are plotted in Fig. 7 as a function of IPD. The normalization factor was the maximum value of each derivation as a function of IPD. The minimum value in some cases was so small that it seems unreasonable to be used as a normalization factor.

Two types of architectures were tested: combined right and left EE cells and combined right and left EI cells. Each of the architectures was tested by both types of coding rate and AIN. As expected, all the different models yielded a similar behavior, a minimum at $\text{IPD} = 0°$ and a symmetric increase with $|\text{IPD}|$.

The results presented in Fig. 7 cannot indicate which of the four models are most appropriate to predict the psychoacoustical measurements. However, the results shown in Fig. 7 were obtained by using an optimum ipsilateral phase delay. Since only EE cells according to AIN coding provide a reasonable match between the physiological experimental re-

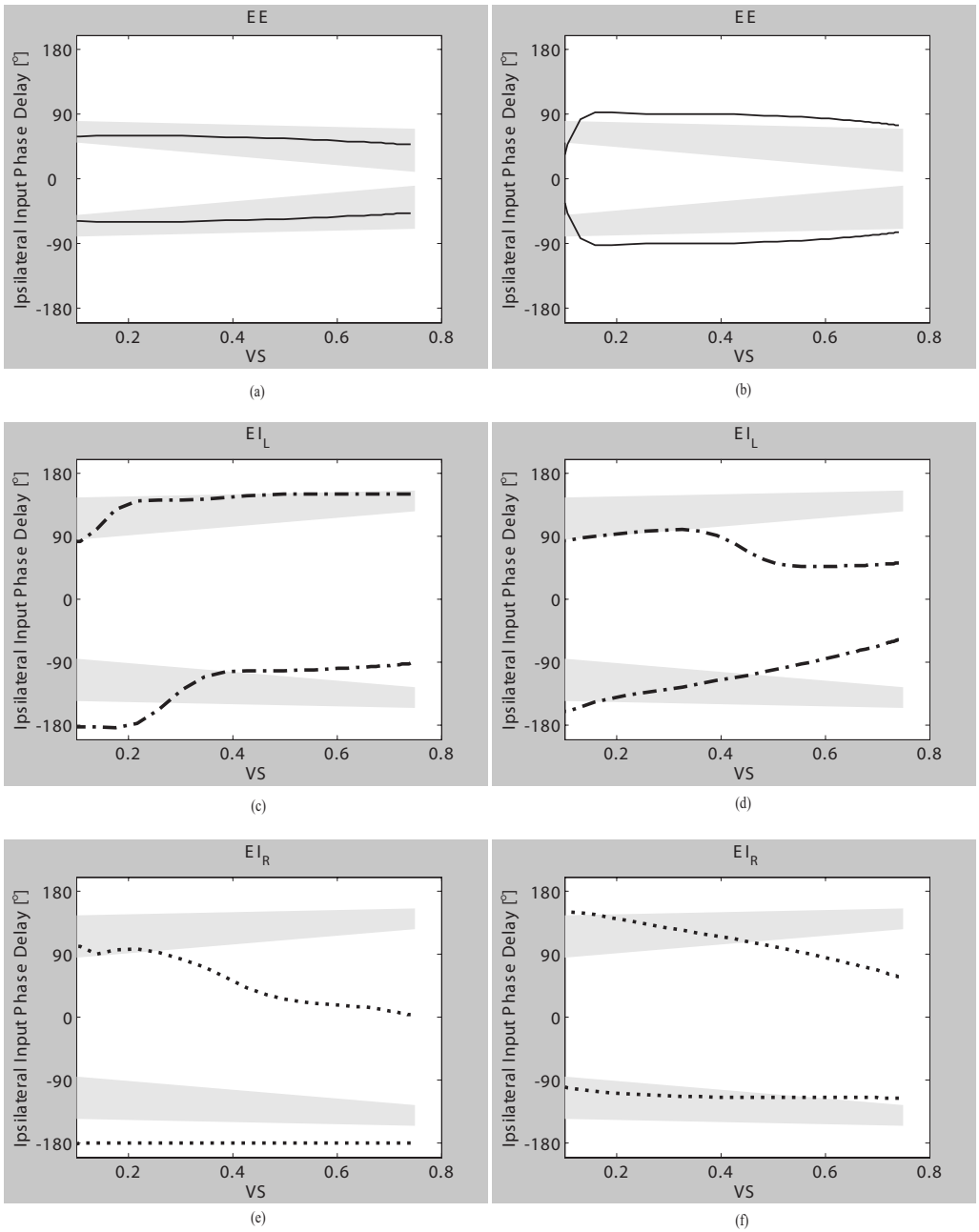

FIG. 6. The derived optimal ipsilateral input phase delay as a function of VS. The theoretical calculations are denoted by the solid lines, and the physiological data are denoted by the gray shadowed areas. Each panel represents a different model as follows: (a) EE cell and AIN coding, (b) EE cell and rate coding, (c) left EI cell and AIN coding, (d) left EI cell and rate coding, (e) right EI cell and AIN coding, and (f) right EI cell and rate coding.

sults (Fig. 6), we conclude that the combined EE cells with AIN coding are the most appropriate to predict the psychoacoustical data.

B. Prediction of interaural level difference

Figure 1 represents the architecture of EE and EI cells that are used for predicting ILD. For simplicity, we define the binaural stimulus with no IPDs, which yields

$$S_L(t) = A_L \sin(2\pi f t),$$
$$S_R(t) = A_R \sin(2\pi f t). \tag{23}$$

Deriving $\lambda_{EE}(t,\mathrm{ILD})$ and $\lambda_{EI}(t,\mathrm{ILD})$ by substituting Eqs. (23) and (19) in Eqs. (11) and (12) reveals that both IRs can be expressed as a multiplication of two functions, where one depends on ILD only and the other one on the time only, i.e.,

$$\lambda_{EE}(t,\mathrm{ILD}) = f_1(\mathrm{ILD}) f_2(t),$$
$$\lambda_{EI}(t,\mathrm{ILD}) = f_3(\mathrm{ILD}) f_4(t). \tag{24}$$

Substituting Eq. (24) in the expressions for the rate CRLB (Eq. (3)) and AIN CRLB (Eq. (5)) reveals an equal value, i.e.,

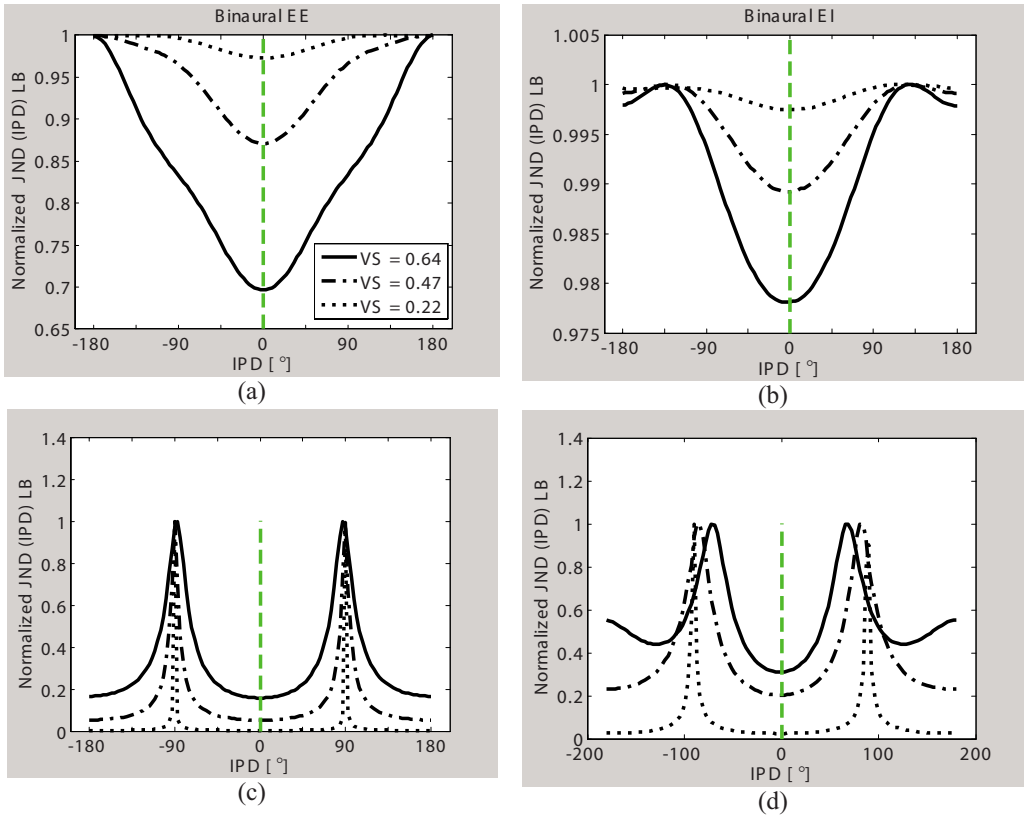

FIG. 7. (Color online) Normalized lower bound of JND as a function of IPD according to the following models: (a) combined right and left EE cells and AIN coding, (b) combined right and left EI cells and AIN coding, (c) combined right and left EE cells and rate coding, and (d) combined right and left EI cells and rate coding.

$$\left.\begin{aligned}\mathrm{CRLB}_{\mathrm{RATE}}^{\mathrm{EE}}(\mathrm{ILD}) &= \mathrm{CRLB}_{\mathrm{AIN}}^{\mathrm{EE}}(\mathrm{ILD}) \\ &= \left\{\frac{1}{f_1(\mathrm{ILD})}\left(\frac{\partial f_1(\mathrm{ILD})}{\partial \mathrm{ILD}}\right)^2 \int_0^T f_2(t)dt\right\}^{-1/2} \\ \mathrm{CRLB}_{\mathrm{RATE}}^{\mathrm{EI}}(\mathrm{ILD}) &= \mathrm{CRLB}_{\mathrm{AIN}}^{\mathrm{EI}}(\mathrm{ILD}) \\ &= \left\{\frac{1}{f_3(\mathrm{ILD})}\left(\frac{\partial f_3(\mathrm{ILD})}{\partial \mathrm{ILD}}\right)^2 \int_0^T f_4(t)dt\right\}^{-1/2}\end{aligned}\right\}. \tag{25}$$

Figure 8 represents the normalized average rates $\bar{\lambda}_{\mathrm{EE}}$ and $\bar{\lambda}_{\mathrm{EI}}$ as functions of ILD for different input frequencies. The spiking rate is normalized so that the sum of the average spiking rate in both AN is equal to 400 spikes/s (e.g., when the amplitude is equal, the average spiking rate for both ears equals 200 spikes/s). Since both right and left EE cells are identical, the normalized average rate of an EE cell is presented in a single figure [Fig. 8(a)] as a function of ILD, which yields a maximum when both inputs are in phase (ILD=0) and decreases as |ILD| increases. In general, a similar behavior was obtained for all input frequencies.

In the simulation shown in Fig. 8, we used $\Delta=20$ μs for EE cells and $\Delta=200$ μs for EI cells similar to the ITD simulation. The left and right EI cells demonstrate a monotonic change with ILD. Right and left SOCs are antisymmetric relative to each other [Figs. 8(b) and 8(c)]. The inhibitory input arrives from the ipsilateral ear, while the excitatory input arrives from the contralateral ear. $\bar{\lambda}_{\mathrm{EI}}^{(R)}$ and $\bar{\lambda}_{\mathrm{EI}}^{(L)}$ yield a minimum when the ipsilateral signal is the strongest and the contralateral is the weakest.

The behavior of the EI mean output spiking rate resembles experimental data in the midlevel range, a monotonic linear increase as a function of ILD in the contralateral EI. EE, on the other hand, produces an artificial ambiguity (signals approaching with either positive or negative ILD obtain equal spiking rates), which is not solved as for ITD since there is no parallel biological mechanism in the ILD processing to the phase shift at the ITD neural mechanisms. EI cells produce an antisymmetric response which is ambiguity-free even when using a single-side SOC. Moreover, the result of the EI cells' mean rate as a function of VS is negligible.

Equation (25) shows that the performance bound (CRLB ILD) when using either rate or AIN model is identical; thus there is no need for the brain to use timing information for ILD extraction. With this information there is no need to plot the CRLB(ILD) using both models. CRLB(ILD) predictions are presented as a function of ILD in Fig. 9. Since $\lambda_{\mathrm{EE}}^{(R)}(t,\mathrm{ILD})=\lambda_{\mathrm{EE}}^{(L)}(t,\mathrm{ILD})$, both right and left EE cells provide identical behaviors that correspond to EE. Right and left EI cells, on the other hand, provide different behaviors, as can be seen in Figs. 9(a) and 9(b).

EE cells yield a maxima at ILD=0 dB. This behavior was found for all frequencies (see Eq. (25)). Right and left EI cells provided an antisymmetric behavior between left and

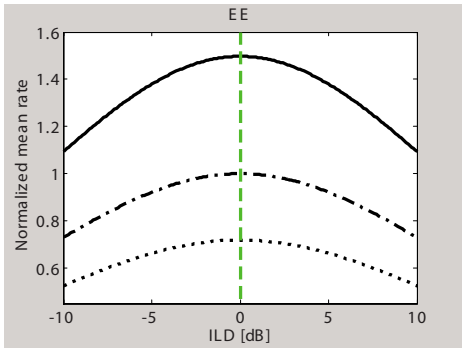

(a)

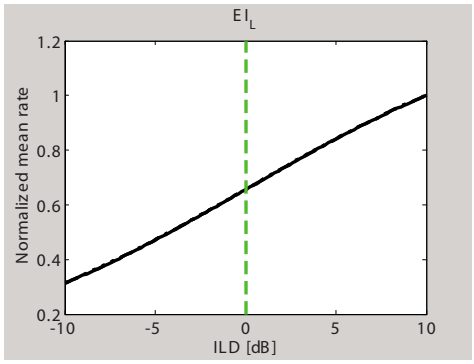

(b)

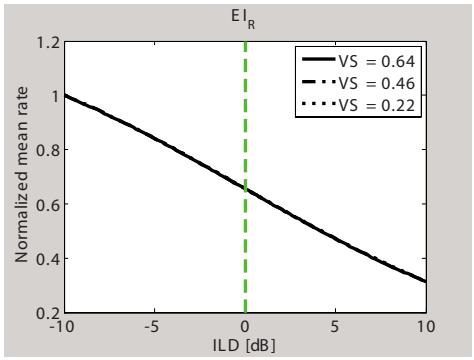

(c)

FIG. 8. (Color online) Normalized mean rate as a function of ILD for different frequencies (indicated by their VS) as obtained by the following types of cells: (a) EE, (b) left EI, and (c) right EI. In each panel, the normalization factor is equal to the maximum value.

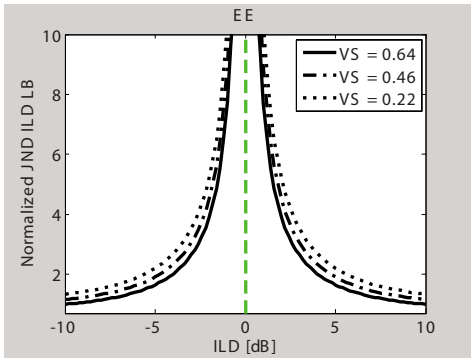

(a)

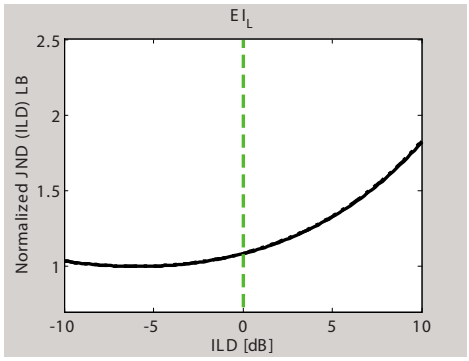

(b)

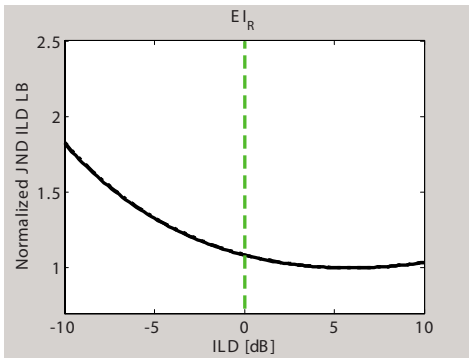

(c)

FIG. 9. (Color online) Normalized lower bound of JND of ILD as a function of ILD derived by (a) EE cell, (b) left EI cell, and (c) right EI cell. Each curve represents a different input frequency as indicated by its VS. In each panel, the normalization factor is equal to the minimum value

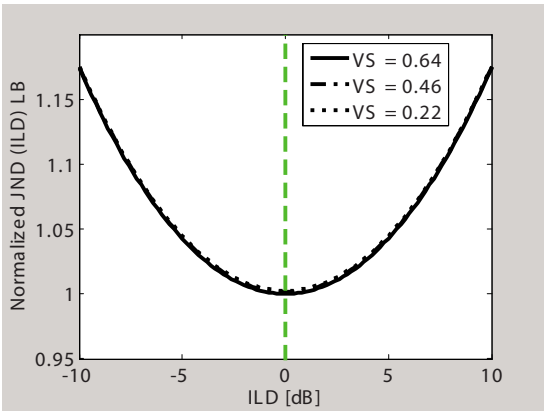

FIG. 10. (Color online) Normalized lower bound of JND as a function of ILD according to combined right and left EI cells for different frequencies as indicated by their VS.

right. This was expected in view of the mean rate behavior (Fig. 8), which fully determines the performance for ILD stimuli.

In order to predict the psychoacoustical results, we combined the information from both sides as expressed in Eq. (13). We expect a minimum JND at ILD=0 dB and a symmetric increase in JND with an absolute increase in ILD (Furst and Algom, 1995). The resulting JND(ILD) is plotted in Fig. 10 for EI cells, whereas the normalized JND(ILD) bound for EE cells is identical to that plotted for monaural EE cells at Fig. 9(a) and found as not adequate. Since the JND of EE cell reached infinity at ILD=0, The JND was normalized to the minimum value. As can be seen, EI predictions resemble the experimental results, a minimum at ILD=0 dB and a symmetric increase with |ILD|. The identical behavior of the bound both for rate and all-information models demonstrates the robustness of the mechanisms especially to injuries that might even harm the synchronization of the signals. The response across frequencies is essential for creating a robust mechanism that can integrate data across frequencies and cope with high-frequency signals with a large bandwidth.

C. Minimal audible angle

In order to evaluate the ability of EE and EI cells to predict the minimum perceived azimuth direction of sine waves, the input signal should be convolved with HRTF [Eq. (14)]. In the following simulation, a typical set of HRTF was used. It was obtained from a "Knowles Electronic Manikin for Auditory Research" (KEMAR) on a dummy head (Algazi *et al.*, 2001).

As suggested by Eq. (15), due to HRTF, both ITD and ILD are affected. Thus, in evaluating the MAA, both ITD and ILD should be considered. According to the previous sections, ITD was best described by EE and AIN coding, while ILD was best coded by EI cells where both rate and AIN codings provided identical behaviors. Therefore when MAA is considered, we shall refer to AIN coding only, which will cover both ITD and ILD.

MAA will be tested as a function of frequency. As was mentioned earlier, the frequency dependence is uniquely determined by VS [Eq. (21)]. Figure 11 represents CRLB-(MAA) as a function of frequency for frontal direction (facing the nose) according to AIN coding for both EE and EI cells. All the derivations were obtained from the two sides of the brain (right and left) according to Eq. (13) and are indicated as binaural EE and binaural EI in Fig. 11.

Each curve in Fig. 11 represents a different VS, as indicated by the parameter β in Eq. (21). The curve that represents an input that lost its synchrony at relatively high frequencies (β=0.0001, solid line) reveals a decrease in MAA as a function of frequency. On the other hand, synchrony loss at low frequencies (β=0.0007, dotted line) reveals an increase in MAA as a function of frequency by both EE and EI cells. However, experimental data demonstrate generally improving performance at low frequencies and deteriorating performance at high frequencies with minimal performances at about 2 and 8 kHz (Mills, 1958). None of those experimental results were predicted by CRLB.

It is quite possible that CRLB failed to predict the MAA experimental results due to the fact that it uses only local information of the parameter under test. Human sound localization, on the other hand, is inherently ambiguous; this requires consideration of other possible parameters other than the true.

The BLB seems to be the most appropriate for the purpose of evaluating performance while taking into consideration other possibilities of the estimated parameter in addition to the true one. BLB was derived in Appendix A, and

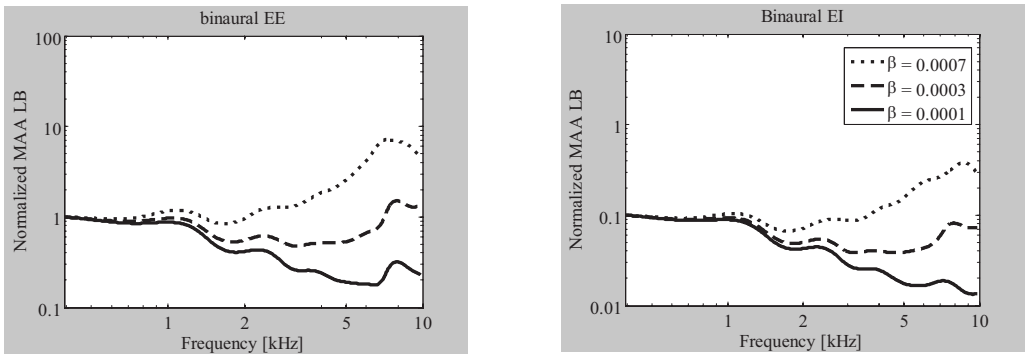

(a) (b)

FIG. 11. Normalized CRLB of MAA as a function of frequency obtained by binaural EE and binaural EI cells. The different curves represent various VS functions [Eq. (21)] that are denoted by the parameter β.

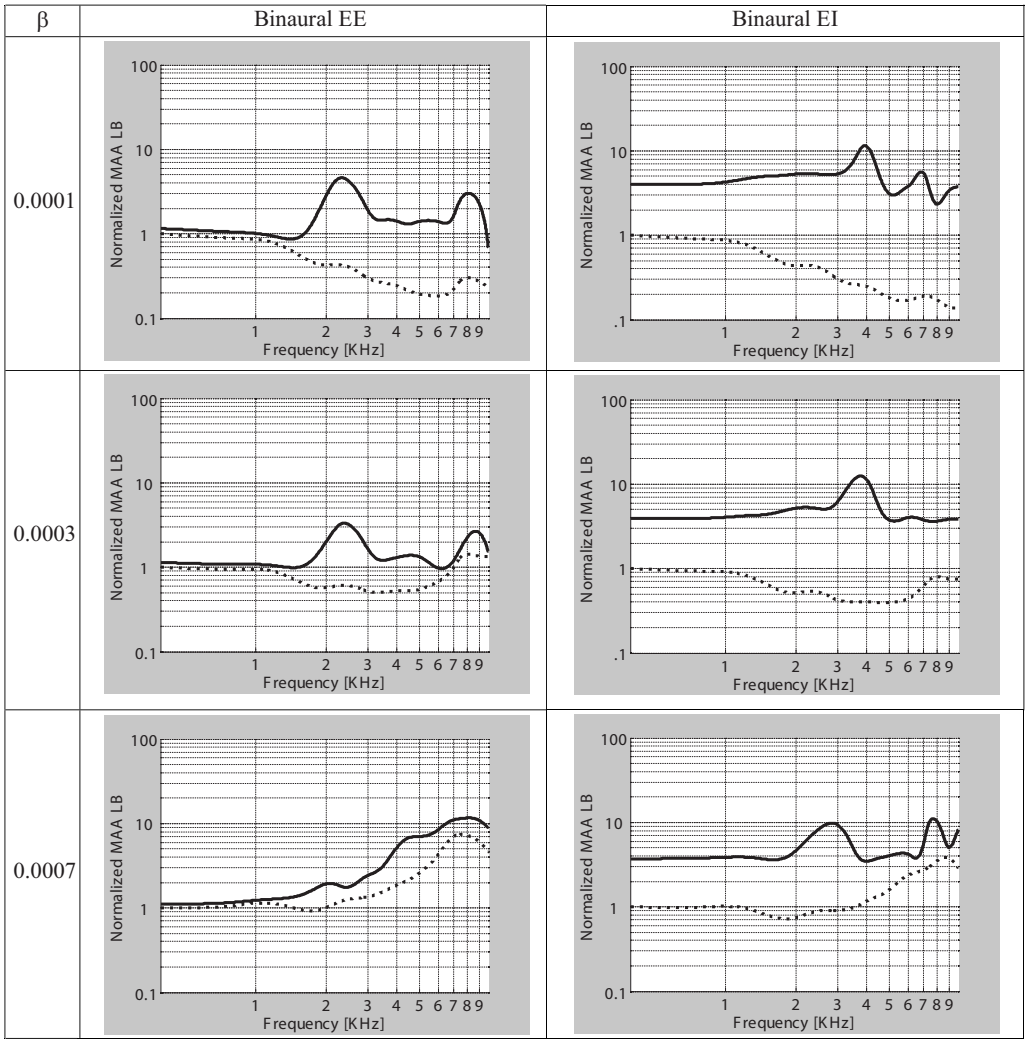

FIG. 12. Normalized BLB (solid line) and CRLB (dotted line) of MAA as a function frequency, obtained from binaural EE cells (left panels) and binaural EI cells (right panels). Each row represents a different VS function [Eq. (21)] and is indicated by the parameter β.

the final results are given in Eqs. (6)–(8). For every tested frequency other directions than the frontal reference direction were taken into account. For all the frequencies, the back-front confusion was included by adding to the true reference $\theta=0°$, the opposite direction $\theta=180°$. Moreover, there were frequencies that yielded more ambiguous directions as was obtained from the HRTF. For example, a signal of 2 kHz that arrives from the front of a subject's face ($\theta=0°$) can be confused with signals coming from the back ($\theta=180°$) and from both sides ($\theta=\pm 90°$). Therefore, in Eqs. (6)–(8), $L=3$, and $\underline{\alpha}=[-90°, 90°, 180°]$.

Figure 12 represents both lower bounds, CRLB (dotted lines) and BLB (solid lines), as functions of frequency as derived by both binaural EE and EI cells. There are six panels in Fig. 12. The left panels represent the binaural EE cells, and the right panels represent the binaural EI cells. Each row represents a different VS function corresponding to those presented in Fig. 11. As expected, BLB yielded higher values than CRLB for all the cases. The greatest difference between BLB and CRLB was obtained for $\beta=0.0001$ (synchrony loss at high frequencies). For EE cells, BLB yielded local maxima at frequencies that are perceived similarly when coming from several directions such as 2.5 and 8 kHz. CRLB, on the other hand, yielded a monotonic decrease for frequencies below 2 kHz. The oscillatory behavior was also obtained by EI cells, but the local maxima were obtained at around 4 and 7 kHz.

Decreasing the frequency for which the input auditory nerve loses its synchrony (increasing β) reveals an increase in MAA predictions by both CRLB and BLB for EE cells. Yet, EI cells maintained an oscillatory behavior for this case as well.

From this simulation it is quite clear that the oscillatory behavior in MAA experimental data (Mills, 1958) is due to the physical acoustical ambiguity of sine waves that affect perception. Both EE and EI cells produced such behavior. The amount of oscillation and the frequencies that yield the worst performances depend on the function that describes the synchrony loss in the auditory nerve. Since this function is unknown in the human auditory nerve, we cannot uniquely determine if EE cells, EI cells, or both are adequate for describing human abilities in MAA experiments.

IV. DISCUSSION

We have investigated the ability of EE and EI CD cells to provide the required acoustical cues (ITD and ILD) and

the source angle for binaural localization. Our study was based on the analytical derivation of the IRs of EE and EI cells whose inputs are NHPP. The ability of EE and EI cells to estimate the input of acoustical cues was analyzed by analytically computing the lower bounds of estimator variances and comparing them to binaural behavioral performances. We compared two types of possible neural coding: (1) rate coding that ignores spike timing information and (2) AIN (all-information) coding that considers spike timing occurrences.

Our simulation revealed the following main results:

(1) Behavioral ITD can be estimated by either EE or EI cells while using any type of coding method only if the ipsilateral input exhibits a phase delay.
(2) Only when EE cells use AIN coding does the optimal derived ipsilateral phase delay match physiological results (Yin and Chan, 1990; Palmer *et al.*, 2002; McAlpine and Grothe, 2003; Hancock and Delgutte, 2004; Joris and Yin, 2006), i.e., a phase delay between 40° and 65°. We thus concluded that ITD is primarily estimated by EE cells when firing timing information is considered.
(3) In deriving the lower bounds for ILD, both types of coding yielded identical results. We thus concluded that for ILD, firing timing information is redundant and rate coding is sufficient.
(4) Only analysis of EI cells revealed an asymmetric response for positive and negative ILDs as found in physiological experiments (Yin and Chan, 1990; Palmer *et al.*, 2002; Park, 1998). Analysis of EE cells yielded a symmetric response that does not match experimental results. We thus conclude that ILD is primarily estimated by EI cells according to rate coding.
(5) In the MAA derivation, the BLB was found as a better estimate than the CRLB. This is due to the fact that the BLB also takes into account ambiguous directions other than the true direction, while CRLB relates only to the true direction.
(6) Following the BLB derivation of MAA, both EE and EI cells revealed an oscillatory performance of MAA as a function of frequency as was found behaviorally (Stevens and Newman, 1934; Mills, 1958; Harris, 1972).

We have tested EE and EI cell performances only for single tones. For ITD estimation, we have shown in the simulation that the CD cells efficiently perform correlation for single tones. However, the analytical expressions for the IRs of EE and EI cells reveal that correlation will be obtained for any input signal. In particular, wide-band signals will yield even better performance since they include more information. Comparing localization of wide-band signals and high-frequency single tones, the former seems to be an easier task than the latter. High-frequency localization suffers from a significant ambiguity problem, but in wide-band signals, EE and EI cells can use additional information such as the signal's envelope that includes low frequencies (Joris and Yin, 1995; Joris, 1996).

Our main results are in general agreement with previous models that included CD cells and modeled binaural abilities, either those that referred to EE cells or those that refer to EI cells and modeled both ITD and ILD (e.g., Lindemann, 1986; Stern and Trahiotis, 1995; Colburn, 1996; Yue and Johnson, 1997; McAlpine *et al.*, 1998; Breebaart *et al.*, 2001; Palmer *et al.*, 2002; Colburn *et al.*, 2004; Park *et al.*, 2004). However, the methodology presented in this paper was proven to be very efficient in determining brainstem neural coding constraints. The use of analytical expressions for the IRs of both EE and EI cells makes it possible to straightforwardly compare the performances of both rate and AIN codings.

The synchrony function of the human auditory nerve (Rose *et al.*, 1967; Johnson, 1980; Palmer and Russell, 1986; Joris *et al.*, 1994; McAlpine *et al.*, 2001; Fitzpatrick and Kuwada, 2001) is still an open question. Using MAA predictions, we have shown that localization performances depend on the synchrony function. The methodology presented in this paper, which takes into account the ambiguity in source localization along with experimental MAA data from different reference positions, might help resolve this issue.

The analysis presented in this paper highlights some interesting points regarding the efficiency of the brain's signal processing. For instance, ITD is estimated by EE cells when all information (AIN model) is considered; it is particularly relevant for low frequencies in the midrange levels where the auditory nerve response is phase locked. For high frequencies, the auditory nerve response is not synchronized, and thus ITD evaluation is not efficient. In examining the MAA predictions as presented in this paper, we saw that the acoustic ambiguity due to human head size causes deterioration in MAA performance even if the auditory nerve would have been phase locked (Krips and Furst, 2006b). Thus it seems that the human brain does not "waste energy" on encoding high-frequency timing information since the performance deteriorates due to ambiguity.

Another interesting point is that for ILD estimation the timing information can be ignored. Therefore AIN and rate codings provide identical performances. Even for low frequencies, AIN is not required for estimating ILD. It seems that the human brain does not restore information that does not provide any significant advantages from the perspective of timing and level of performance.

All the calculations in the present paper used a single cell in each side of the brain. Therefore, the data were normalized, and only a qualitative comparison compared to experimental results was obtained. A quantitative comparison will only be possible when a complete model of SOC and its preceding brainstem neural nuclei will be available. In particular, it should include a number of EE and EI cells and their frequency phase-locking characteristics, including level-dependent properties. However, the methodology used in this paper is adequate for further investigations that will focus on other auditory brainstem source phenomena.

ACKNOWLEDGMENT

This research was partly supported by the Adams Brain Center at Tel Aviv University.

APPENDIX A: BARANKIN LOWER BOUND DERIVATION OF A NONHOMOGENEOUS POISSON PROCESS

Barankin (1949) developed a lower bound that takes into account different possible values of the estimated parameter other than those located in the proximity of the true one (ambiguous locations). If the true value is α^* and there are L other possible values $\alpha_1,\ldots,\alpha_L \neq \alpha^*$, then the BLB was derived and is obtained by

$$\sigma(\hat{\alpha}) \geqslant \mathrm{BLB}(\alpha^*) = \sqrt{[\mathrm{CRLB}(\alpha^*)]^2 + \underline{\Gamma}(\alpha^*)\Delta^{-1}(\alpha^*)\underline{\Gamma}^T(\alpha^*)}, \quad \text{(A1)}$$

where $\underline{\Gamma}(\alpha^*)=\underline{\alpha}-\mathrm{CRLB}^2(\alpha^*)\underline{A}$ and $\Delta(\alpha^*)=B-\underline{A}^T\mathrm{CRLB}^2(\alpha^*)\underline{A}$. $\mathbf{B}$ is a symmetric matrix whose size is $L\times L$, and $\underline{\alpha}$ and $\underline{A}$ are vectors with size L ($\underline{\alpha}=[\alpha_1,\ldots,\alpha_L]$, $\underline{A}=[A_1,\ldots,A_L]$).

McAulay and Hofstetter (1971) showed that for a single parameter vector $\underline{\mathbf{A}}$ elements are given by

$$A_p = \sum_{n=0}^{N}\int_{t_1=0}^{T}\int_{t_2=0}^{T}\cdots\int_{t_n=0}^{T}\frac{\partial \ln[P(t_1,\ldots,t_n|\alpha^*)]}{\partial\alpha} \times P(t_1,\ldots,t_n|\alpha_p)dt_1,\ldots,dt_n, \quad 1\leqslant p\leqslant L, \quad \text{(A2)}$$

and the matrix $\mathbf{B}$ elements are given by

$$B_{ij} = \sum_{n=0}^{N}\int_{t_1=0}^{T}\int_{t_2=0}^{T}\cdots\int_{t_n=0}^{T}\frac{P(t_1,\ldots,t_n|\alpha_i)}{P(t_1,\ldots,t_n|\alpha^*)} \times P(t_1,\ldots,t_n|\alpha_j)dt_1,\ldots,dt_n, \quad \begin{matrix}1\leqslant i\leqslant L\\ 1\leqslant j\leqslant L\end{matrix}. \quad \text{(A3)}$$

In rate coding, the probability $P(t_1,\ldots,t_n|\alpha)=P_{\mathrm{rate}}(N(0,T)=n|\alpha)$, as defined in Eq. (2), which yields

$$\frac{\partial \ln(P(N(0,T)=n|\alpha))}{\partial\alpha} = \frac{n\int_0^T\frac{\partial\lambda(t,\alpha)}{\partial\alpha}dt}{\int_0^T\lambda(t,\alpha)dt} - \int_0^T\frac{\partial\lambda(t,\alpha)}{\partial\alpha}dt. \quad \text{(A4)}$$

Substituting Eqs. (A3) and (2) in Eq. (A2) yields

$$A_p^{\mathrm{rate}} = \sum_{n=0}^{N}\left[\frac{n\int_0^T\frac{\partial\lambda(t,\alpha)}{\partial\alpha^*}dt}{\int_0^T\lambda(t,\alpha^*)dt} - \int_0^T\frac{\partial\lambda(t,\alpha)}{\partial\alpha^*}dt\right]\frac{1}{n!} \times\left[\int_0^T\lambda(t,\alpha_p)dt\right]^n e^{-\int_0^T\lambda(t,\alpha_p)dt}, \quad 1\leqslant p\leqslant L \quad \text{(A5)}$$

Note that $\Sigma_{n=0}^{N}P_{\mathrm{rate}}(N(0,T)=n|\alpha_p)=1$, and for large N, $\Sigma_{n=0}^{N}P_{\mathrm{rate}}(N(0,T)=n-1|\alpha_p)\to 1$. Thus Eq. (A5) becomes

$$A_p^{\mathrm{rate}} = \int_0^T\frac{\partial\lambda(t,\alpha^*)}{\partial\alpha}dt\left[\frac{\int_0^T\lambda(t,\alpha_p)dt}{\int_0^T\lambda(t,\alpha^*)dt}-1\right], \quad 1\leqslant p\leqslant L. \quad \text{(A6)}$$

Similarly the elements of matrix $\mathbf{B}$ are obtained by substituting Eq. (2) in Eq. (A2), which yields

$$B_{ij} = \sum_{n=0}^{N}\left\{\frac{\int_0^T\lambda(t,\alpha_i)dt}{\int_0^T\lambda(t,\alpha^*)dt}\int_0^T\lambda(t,\alpha_j)dt\right\}^n \times\exp\left\{-\int_0^T\lambda(t,\alpha_i)dt-\int_0^T\lambda(t,\alpha_j)dt + \int_0^T\lambda(t,\alpha^*)dt\right\}, \quad \begin{matrix}1\leqslant i\leqslant L\\ 1\leqslant j\leqslant L\end{matrix} \quad \text{(A7)}$$

For large N, the sum in Eq. (A7) can be expressed as an exponent ($\Sigma_{n=0}^{\infty}(a^n/n!)=e^a$), which yields

$$B_{i,j}^{\mathrm{rate}} = \exp\left(\int_0^T[-\lambda(t,\alpha_i)-\lambda(t,\alpha_j)+\lambda(t,\alpha^*)]dt + \frac{\int_0^T\lambda(t,\alpha_i)dt}{\int_0^T\lambda(t,\alpha^*)dt}\int_0^T\lambda(t,\alpha_j)dt\right). \quad \text{(A8)}$$

In AIN coding, the probability $P(t_1,\ldots,t_n|\alpha)=P_{\mathrm{AIN}}(t_1,\ldots,t_n|\alpha)$, as defined in Eq. (4), which yields

$$\frac{\partial \ln[P(t_1,\ldots,t_n|\alpha^*)]}{\partial\alpha} = \sum_{i=1}^{n}\frac{\partial\lambda(t_i,\alpha^*)}{\partial\alpha}\frac{1}{\lambda(t_i,\alpha^*)} - \int_0^T\frac{\partial\lambda(t,\alpha^*)}{\partial\alpha}dt. \quad \text{(A9)}$$

Substituting Eqs. (A9) and (4) in Eq. (A2) yields an expression for A_p, $A_p^{\mathrm{AIN}}=A_p^{(1)}-A_p^{(2)}$, where

$$A_p^{(1)} = \sum_{n=1}^{N}\sum_{i=1}^{n}\int_{t_1=0}^{T}\int_{t_2=0}^{T}\cdots\int_{t_n=0}^{T}\Upsilon(t_1,\ldots,t_n)dt_1,\ldots,dt_n, \quad \text{(A10)}$$

$$\Upsilon(t_1,\ldots,t_n) = \frac{\partial\lambda(t_i,\alpha^*)}{\partial\alpha}\frac{1}{\lambda(t_i,\alpha^*)} \times\left[\frac{\prod_{k=1}^{n}\lambda(t_k,\alpha_p)}{n!}\exp\left\{-\int_0^T\lambda(t,\alpha_p)dt\right\}\right].$$

Note that the sum in $A_p^{(1)}$ starts at $n=1$ since $n=0$ does not exist in Eq. (A9) and

$$A_p^{(2)} = \sum_{n=0}^{N} \int_{t_1=0}^{T} \int_{t_2=0}^{T} \cdots \int_{t_n=0}^{T} \left[\int_0^T \frac{\partial \lambda(t,\alpha^*)}{\partial \alpha} dt \right] \times \left[\frac{\prod_{k=1}^{n} \lambda(t_k,\alpha_p)}{n!} \exp\left\{ - \int_0^T \lambda(t,\alpha_p) dt \right\} \right] dt_1, \ldots, dt_n. \quad \text{(A11)}$$

Let us denote $P_{\mathrm{AIN}}(n-1\,|\,\alpha)$ as the AIN probability when $N(0,T)=n-1$ and substituting it in Eq. (A10), which yields

$$A_p^{(1)} = \sum_{n=1}^{N} \sum_{i=1}^{n} \int_{t=0}^{T} \frac{\partial \lambda(t,\alpha^*)}{\partial \alpha} \frac{\lambda(t,\alpha_p)}{\lambda(t,\alpha^*)} dt \frac{P_{\mathrm{AIN}}(n-1|\alpha_p)}{n}. \quad \text{(A12)}$$

Replacing the order of the sums and integration yields

$$A_p^{(1)} = \sum_{n=1}^{N} \frac{P_{\mathrm{AIN}}(n-1|\alpha_p)}{n} \sum_{i=1}^{n} \int_{t=0}^{T} \frac{\partial \lambda(t,\alpha^*)}{\partial \alpha} \frac{\lambda(t,\alpha_p)}{\lambda(t,\alpha^*)} dt. \quad \text{(A13)}$$

Since $\int_{t=0}^{T} (\partial \lambda(t,\alpha^*)/\partial \alpha)(\lambda(t,\alpha_p)/\lambda(t,\alpha^*))dt$ is independent both of i and n, $A_p^{(1)}$ can be expressed as

$$A_p^{(1)} = \int_{t=0}^{T} \frac{\partial \lambda(t,\alpha^*)}{\partial \alpha} \frac{\lambda(t,\alpha_p)}{\lambda(t,\alpha^*)} dt \sum_{n=1}^{N} \frac{P_{\mathrm{AIN}}(n-1|\alpha_p)}{n} n. \quad \text{(A14)}$$

For large N, $\Sigma_{n=1}^{N} P(n-1\,|\,\alpha) \to 1$; thus

$$A_p^{(1)} = \int_{t=0}^{T} \frac{\partial \lambda(t,\alpha^*)}{\partial \alpha} \frac{\lambda(t,\alpha_p)}{\lambda(t,\alpha^*)} dt. \quad \text{(A15)}$$

Similarly $A_p^{(2)}$ can be expressed as

$$A_p^{(2)} = \int_0^T \frac{\partial \lambda(t,\alpha^*)}{\partial \alpha} dt \sum_{n=0}^{N} \left(\int_{t_1=0}^{T} \int_{t_2=0}^{T} \cdots \int_{t_n=0}^{T} \frac{\prod_{k=1}^{n} \lambda(t_k,\alpha_p)}{n!} \times \exp\left\{ - \int_0^T \lambda(t,\alpha_p) dt \right\} dt_1, \ldots, dt_n \right). \quad \text{(A16)}$$

The second element in Eq. (A16) is the sum over all the possible discharge possibilities, i.e., $(\Sigma_{n=0}^{N} P_{\mathrm{AIN}}(n|\alpha)=1)$. Hence $A_p^{(2)}$ is given by

$$A_p^{(2)} = \int_0^T \frac{\partial \lambda(t,\alpha^*)}{\partial \alpha} dt. \quad \text{(A17)}$$

Substituting Eqs. (A15) and (A17) in the expression for A_p^{AIN} yields

$$A_p^{\mathrm{AIN}} = \int_0^T \frac{\partial \lambda(t,\alpha^*)}{\partial \alpha} \frac{\lambda(t,\alpha_p)}{\lambda(t,\alpha^*)} dt - \int_0^T \frac{\partial \lambda(t,\alpha^*)}{\partial \alpha} dt. \quad \text{(A18)}$$

Similarly, the elements in matrix **B** each are given by

$$B_{i,j}^{\mathrm{rate}} = \exp\left\{ - \int_0^T [\lambda(t,\alpha_i) + \lambda(t,\alpha_j) - \lambda(t,\alpha^*)] dt \right\} \times \sum_{n=0}^{N} \frac{1}{n!} \left(\int_{t=0}^{T} \frac{\lambda(t,\alpha_i)\lambda(t,\alpha_j)}{\lambda(t,\alpha^*)} dt \right)^n. \quad \text{(A19)}$$

For large N, the sum in Eq. (A19) can be expressed as an exponent $(\Sigma_{n=0}^{\infty}(a^n/n!)=e^a)$, which yields

$$B_{i,j}^{\mathrm{AIN}} = \exp\left(\int_0^T \left[- \lambda(t,\alpha_i) - \lambda(t,\alpha_j) + \lambda(t,\alpha^*) + \frac{\lambda(t,\alpha_i)\lambda(t,\alpha_j)}{\lambda(t,\alpha^*)} \right] dt \right). \quad \text{(A20)}$$

Agmon-Snir, H., Carr, C. E., and Rinzel, J. (**1998**). "The role of dendrites in auditory coincidence detection," Nature (London) **393**, 268–272.

Algazi, V. R., Duda, R. O., Thompson, D. M., and Avendano, C. (**2001**). "The CIPIC HRTF database," IEEE Workshop on the Applications of Signal Processing to Audio and Acoustics, pp. 99–102.

Bar David, I. (**1969**). "Communication under Poisson regime," IEEE Trans. Inf. Theory **IT-15**, 31–37.

Barankin, E. W. (**1949**). "Locally best unbiased estimates," Ann. Math. Stat. **20**, 477–501.

Batra, R., Kuwada, S., and Fitzpatrick, D. C. (**1997**). "Sensitivity to interaural temporal disparities of low- and high-frequency neurons in the superior olivary complex. I. Heterogeneity of responses," J. Neurophysiol. **78**, 1222–1236.

Blauert, J. (**1997**). *Spatial Hearing: The Psychophysics of Human Sound Localization* (MIT, London).

Boudreau, J. C., and Tsuchitani, C. (**1968**). "Binaural interaction in the cat superior olive S segment," J. Neurophysiol. **31**, 442–454.

Boudreau, J., and Tsuchitani, C. (**1970**). "Cat superior olive S-segment cell discharge to tonal stimulation," Contrib Sens Physiol. **4**, 143–213.

Brand, A., Behrend, O., Marquardt, T., McAlpine, D., and Grothe, B. (**2002**). "Precise inhibition is essential for microsecond interaural time difference coding," Nature (London) **417**, 543–547.

Breebaart, J., Van de Par, S., and Kohlrausch, A. (**2001**). "Binaural processing model based on contralateral inhibition. I. Model structure," J. Acoust. Soc. Am. **110**, 1074–1088.

Brown, C. J., and Abbas, P. J. (**1990**). "Electrically evoked whole-nerve action poten tials: Parametric data from the cat," J. Acoust. Soc. Am. **88**, 2205–2210.

Bruce, I. C., Irlicht, L. S., White, M. W., O'Leary, S. J., Dynes, S., Javel, E., and Clark, G. M. (**1999**). "A stochastic model of the electrically stimulated auditory nerve: Pulse-train response," IEEE Trans. Biomed. Eng. **46**, 630–637.

Caird, D. M., and Klinke, R. (**1983**). "Processing of binaural stimuli by cat superior olivary complex neurons," Exp. Brain Res. **52**, 385–399.

Cant, N. B. (**1991**). "Projections to the lateral and medial superior olivary nuclei from the spherical and globular bushy cells of the anteroventral cochlear nucleus," in *Neurobiology of Hearing: The Central Auditory System*, edited by R. A. Altschuler, R. P. Bobbin, B. M. Clopton, and D. W. Hoffman (Raven, New York), pp. 99–119.

Caspary, D. M., and Finlayson, P. G. (**1991**). "Superior olivary complex—Functional neuropharmacology of the principal cell types," in *Neurobiology of Hearing: The Central Auditory System*, edited by R. A. Altschuler, R. P. Bobbin, B. M. Clopton, and D. W. Hoffman (Raven, New York), pp. 141–161.

Cohen, O., Furst, M., and Krips, R., (**2004**). "ITD and ILD estimation based on neural stochastic analysis," Proceedings of the 23rd IEEE Convention of Electrical and Electronics Engineers in Israel, pp. 185–188.

Colburn, S. H. (**1973**). "Theory of binaural interaction based on auditory-nerve data. I. General strategy and preliminary results on interaural discrimination," J. Acoust. Soc. Am. **54**, 1458–1470.

Colburn, H. S. (**1996**). "Computational models of binaural processing," in *Springer Handbook of Auditory Research, Vol. VI: Auditory Computation*, edited by H. L. Hawkins, T. A. McMullen, A. N. Popper, and R. R. Fay (Springer-Verlag, New York).

Colburn, H. S., Zhou, Y., and Dasika, V. K. (**2004**). "Inhibition in models of

coincidence detection," *Auditory Signal Processing: Physiology, Psychoacoustics, and Models* (Springer-Verlag, New York).
Crow, G., Rupert, A. L., and Moushegian, G. (**1978**). "Phase locking in monaural and binaural medullary neurons: Implications for binaural phenomena," J. Acoust. Soc. Am. **64**, 493–501.
Delgutte, B., Joris, P. X., Litovsky, R. Y., and Yin, T. C. (**1999**). "Receptive fields and binaural interactions for virtual-space stimuli in the cat inferior colliculus," J. Neurophysiol. **81**, 2833–2851.
Durlach, N. I., and Colburn, H. S. (**1978**). "Binaural phenomena," in *Handbook of Perception*, edited by E. C. Carterette and M. P. Freidman (Academic, New York), Vol. **4**, pp. 365–466.
Dynes, S. (**1996**). "Discharge characteristics of auditory nerve fibers for pulsatile electrical stimuli," Ph.D. thesis, Massachusetts Institute of Technology, Cambridge, MA.
Fitzpatrick, D. C., and Kuwada, S. (**2001**). "Tuning to interaural time differences across frequency," J. Neurosci. **21**, 4844–4851.
Fitzpatrick, D. C., Kuwada, S., and Batra, R. (**2000**). "Neural sensitivity to interaural time differences: Beyond the Jeffress model," J. Neurosci. **20**, 1605–1615.
Furst, M., and Algom, D. (**1995**). "Lateralization and discrimination of dichotic clicks: Evidence from patients with brainstem lesions and normal cohorts," J. Basic Clin. Physiol. Pharmacol. **6**, 149–171.
Glendenning, K. K., Hutson, K. A., Nudo, R. J., and Masterton, R. B. (**1985**). "Acoustic chiasm. II: Anatomical basis of binaurality in lateral superior olive of cat," J. Comp. Neurol. **232**, 261–285.
Goldberg, J. M., and Brown, P. B. (**1969**). "Response of binaural neurons of dog superior olivary complex to dichotic tonal stimuli: Some physiological mechanisms of sound localization," J. Neurophysiol. **32**, 613–636.
Grantham, D. W. (**1986**). "Detection and discrimination of simulated motion of auditory targets in the horizontal plane," J. Acoust. Soc. Am. **79**, 1939–1949.
Guinan, J. J., Guinan, S. S., and Norris, B. E. (**1972**). "Single auditory units in the superior olivary complex. I. Responses to sounds and classifications based on physiological properties," Int. J. Neurosci. **4**, 101–120.
Hancock, K. E., and Delgutte, B., (**2004**). "A physiologically based model of interaural time difference discrimination," J. Neurosci. **24**, 7110–7117.
Harris, J. D. (**1972**). "A florilegium of experiments on directional hearing," Acta Oto-Laryngol. **298**, 3–26.
Hartmann, W. M., and Rakerd, B. (**1989**). "On the minimum audible angle: A decision theory approach," J. Acoust. Soc. Am. **85**, 2031–2041.
Heinz, M. G., Colburn, H. S., and Carney, L. H. (**2001**). "Evaluating auditory performance limits: I. One-parameter discrimination using a computational model for the auditory nerve," Neural Comput. **13**, 2273–2316.
Huettel, L. G., and Collins, L. M. (**2004**). "Predicting auditory tone-in-noise detection performance: The effects of neural variability," IEEE Trans. Biomed. Eng. **51**, 282–293.
Irvine, D. R. F. (**1986**). *The Auditory Brainstem* (Springer-Verlag, Berlin).
Irvine, D. R. F. (**1992**). "Physiology of the auditory brain stem," in *The Mammalian Auditory Pathway: Neurophysiology*, edited by A. N. Popper and R. R. Fay (Springer, New York), pp. 153–231.
Jeffress, L. A. (**1948**). "A place theory of sound localization," J. Comp. Physiol. Psychol. **41**, 35–39.
Johnson, D. (**1980**). "The relationship between spike rate and synchrony in responses of auditory-nerve fibers to single tones," J. Acoust. Soc. Am. **68**, 1115–1122.
Joris, P. X. (**1996**). "Envelope coding in the lateral superior olive. II. Characteristic delays and comparison with responses in the medial superior olive," J. Neurophysiol. **76**, 2137–2156.
Joris, P. X., Carney, L. H., Smith, P. H., and Yin, T. C. T. (**1994**). "Enhancement of neural synchronization in the anteroventral cochlear nucleus. I. Responses to tones at the characteristic frequency," J. Neurophysiol. **71**, 1022–1036.
Joris, P. X., Smith, P. H., and Yin, T. C. T. (**1998**). "Coincidence detection in the auditory system: 50 years after Jeffress," Neuron **21**, 1235–1238.
Joris, P. X., and Yin, T. C. T. (**1995**). "Envelope coding in the lateral superior olive. I. Sensitivity to interaural time differences," J. Neurophysiol. **73**, 1043–1062.
Joris, P. X., and Yin, T. C. T. (**2006**). "A matter of time: Internal delays in binaural processing," Trends Neurosci. **30**, 70–78.
King, A. J., and Palmer, A. R. (**1983**). "Cells responsive to free-field auditory stimuli in guinea-pig superior colliculus: Distribution and response properties," J. Physiol. (London) **342**, 361–381.
Klumpp, R. G., and Eady, H. R. (**1956**). "Some measurements of interaural time difference thresholds," J. Acoust. Soc. Am. **28**, 859–860.
Knudsen, E. I. (**1982**). "Auditory and visual maps of space in the optic tectum of the owl," J. Neurosci. **2**, 1177–1194.
Knudsen, E. I., and Konishi, M. (**1978**). "A neural map of auditory space in the owl," Science **200**, 795–797.
Krips, R. (**2008**). "Stochastic properties of coincidence-detector neural cells and their implications for binaural perception," Ph.D. dissertation, Tel-Aviv University, Tel-Aviv, Israel.
Krips, R., and Furst, M. (**2006a**). "Probability characteristics of neural coincidence detectors in the brainstem," J. Acoust. Soc. Am. **120**, 3258.
Krips, R., and Furst, M. (**2006b**). "Theoretical MAA estimation based on ambiguity information," ARO MWM.
Kuhn, G. F. (**1987**). "Physical acoustics and measurements pertaining to directional hearing," in *Directional Hearing*, edited by W. A. Yost and G. Gourevitch (Springer, New York), pp. 3–25.
Lindemann, W. (**1986**). "Extension of a binaural cross-correlation model by contralateral inhibition. I. Simulation of lateralization for stationary signals," J. Acoust. Soc. Am. **80**, 1608–1622.
Liu, L. F., Palmer, A. R., and Wallace, M. N. (**2006**). "Phase-locked responses to pure tones in the inferior colliculus," J. Neurophysiol. **95**, 1926–1935.
McAlpine, D., and Grothe, B. (**2003**). "Sound localization and delay lines—Do mammals fit the model?," Trends Neurosci. **26**, 347–350.
McAlpine, D., Jiang, D., and Palmer, A. R. (**2001**). "A neural code for low-frequency sound localization in mammals," Nat. Neurosci. **4**, 396–401.
McAlpine, D., Jiang, D., Shackleton, T. M., and Palmer, A. R. (**1998**). "Convergent input from brainstem coincidence detectors onto delay sensitive neurons in the inferior colliculus," J. Neurosci. **18**, 6026–6039.
McAulary, R. J., and Hofstetter, E. M. (**1971**). "Barankin bounds on parameter estimation," IEEE Trans. Inf. Theory **IT 17**, 669–676.
Miller, C. A., Abbas, P. J., and Robinson, B. K. (**2001**). "Response properties of the refractory auditory nerve fiber," J. Assoc. Res. Otolaryngol. **2**, 216–232.
Mills, A. W. (**1958**). "On the minimum audible angle," J. Acoust. Soc. Am. **30**, 237–246.
Mills, A. W. (**1960**). "Lateralization of high-frequency tones," J. Acoust. Soc. Am. **32**, 132–134.
Moushegian, G., Rupert, A. L., and Gidda, J. S. (**1975**). "Functional characteristics of superior olivary neurons to binaural stimuli," J. Neurophysiol. **38**, 1037–1048.
Palmer, A. R., McAlpine, D., and Jiang, D. (**1997**). "Processing of interaural delay in the inferior colliculus," in *Acoustical Signal Processing in the Central Auditory System*, edited by J. Syka (Plenum, New York), pp. 353–364.
Palmer, A. M., and Russell, I. J. (**1986**). "Phase-locking in the cochlear nerve of the guinea-pig and its relation to the receptor potential of inner hair-cells," Hear. Res. **24**, 1–15.
Palmer, A. R., Shackleton, T. M., and McAlpine, D. (**2002**). "The physiological basis of the binaural masking level difference," Acta. Acust. Acust. **88**, 312–319.
Park, T. J. (**1998**). "IID sensitivity differs between two principal centers in the interaural intensity difference pathway: The LSO and the IC," J. Neurophysiol. **79**, 2416–2431.
Park, T. J., Klug, A., Holinstat, M., and Grothe, B. (**2004**). "Interaural level difference processing in the lateral superior olive and the inferior colliculus," J. Neurophysiol. **92**, 289–301.
Reyes, A. D., Rubel, E. W., and Spain, W. J. (**1996**). "In vitro analysis of optimal stimuli for phase-locking and time-delayed modulation of firing in avian nucleus laminaris neurons," J. Neurosci. **16**, 993–1007.
Rose, J. E., Brugge, J. F., Anderson, D. J., and Hind, J. E. (**1967**). "Phase-locked response to low-frequency tones in single auditory nerve fibers of the squirrel monkey," J. Neurophysiol. **30**, 769–793.
Searle, C. L., Braida, L. D., Davis, M. F., and Colburn, H. S. (**1976**). "Model for auditory localization," J. Acoust. Soc. Am. **60**, 1164–1175.
Semple, M. N., Aitkin, L. M., Calford, M. B., Pettigrew, J. D., and Phillips, D. P. (**1983**). "Spatial receptive fields in the cat inferior colliculus," Hear. Res. **10**, 203–215.
Siebert, W. M. (**1968**). "Stimulus transformation in the peripheral auditory system," in *Recognizing Patterns*, edited by P. A. Kolers and M. Eden (MIT, Cambridge, MA), pp. 104–133.
Snyder, D. L., and Miller, M. I. (**1991**). *Random point Processes in Time and Space* (Springer-Verlag, Berlin).
Spitzer, M. W., and Semple, M. N. (**1995**). "Neurons sensitive to interaural phase disparity in gerbil superior olive: Diverse monaural and temporal

response properties," J. Neurophysiol. **73**, 1668–1690.
Stern, R. M., Jr., and Colburn, H. S. (**1978**). "Theory of binaural interaction based on auditory-nerve data. IV. A model for subjective lateral position," J. Acoust. Soc. Am. **64**, 127–140.
Stern, R. M., and Trahiotis, C. (**1995**). "Models of binaural perception," in *Hearing*, edited by B. C. J. Moore (Academic, New York), pp. 347–386.
Stevens, S. S., and Newman, E. B. (**1934**). "The localization of pure tones," Proc. Natl. Acad. Sci. U.S.A. **20**, 593–596.
Warr, W. B. (**1966**). "Fiber degeneration following lesions in the anteroventral cochlear nucleus of the cat," Exp. Neurol. **23**, 140–155.
Warr, W. B. (**1969**). "Fiber degeneration following lesions in the posteroventral cochlear nucleus of the cat," Exp. Neurol. **23**, 140–155.
Warr, W. B. (**1972**). "Fiber degeneration following lesions in the multipolar and globular cell areas in the ventral cochlear nucleus of the cat," Brain Res. **40**, 247–270.
Yin, T. C., and Chan, J. C. (**1990**). "Interaural time sensitivity in medial superior olive of cat," J. Neurophysiol. **64**, 465–488.
Yin, T. C. T., Chan, J. C. K., and Carney, L. H. (**1987**). "Effects of interaural time delays of noise stimuli on low-frequency cells in the cat's inferior colliculus. III. Evidence for cross-correlation," J. Neurophysiol. **58**, 562–582.
Yue, L., and Johnson, D. H. (**1997**). "Optimal binaural processing based on point process models of preprocessed cues," J. Acoust. Soc. Am. **101**, 982–992.
Zwislocki, J., and Feldman, R. S. (**1956**). "Just noticeable differences in dichotic phase," J. Acoust. Soc. Am. **28**, 860–864.